The tropical hypothesis revisited: Is Pacific countercurrent consolidation the common mechanism of global cooling in interannual, millennial, and orbital time scales?

John H. Duke

Revision 4-October-2011, Climate of the Past Discussions, 6, 905-961, 2010

138 Congdon St., Providence, RI 02906 USA

Correspondence to: J. H. Duke (johnduke@johnduke.com)

Abstract

Pacific countercurrent consolidation (PCC) is proposed to be the common mechanism of El Niño – La Niña mediated climate change in interannual, millenial, and orbital time scales, reflecting operation in a single Earth system. In short time scales, PCC follows a novel hypothesis of El Niño – La Niña forcing in which internal tide resonance dissipates the vorticity that powers northward Sverdrup transport, so the North Equatorial Countercurrent merges geostrophically into the Equatorial Undercurrent. The resulting PCC reduces countercurrent shear surface friction to trigger eastward advection at El Niño onset. ITR is observed in wavelet analysis of one hour resolution western Pacific thermocline temperature, revealing >8°C amplitude resonance in the semidiurnal tide band prior to El Niño onset in 1997, 2002 and 2006. This ITR is independent of westerly wind bursts. Subsequently, persistent PCC prevents warm pool recharge, leading to an equatorially symmetric La Niña mode with global cooling teleconnections. Proposed interannual and millennial time scale cycles in higher tidal force are consistent with instrument and proxy records of global cooling phases. In orbital time scales, mutual precession and obliquity mediated southward migration of the intertropical convergence zone also results in PCC, because the North Equatorial Countercurrent follows the intertropical convergence zone. The mid-Pleistocene transition is evidence of mutual obliquity-precession control, for this is when their phase relationship changes from 1:2 (40 thousand year cycles) to 2:5 or 3:5 (80 or 120 thousand year cycles).

1. Introduction

Earth's climate records reveal periodicities in multiple time scales. The 2 to 7 year El Niño Southern Oscillation (ENSO) (Wang and Picaut, 2004) is the dominant interannual cycle. In the millennial domain, Dansgaard/Oescher and Heinrich events recur in 1 to 2 thousand year (kyr) intervals (Clark et al. eds. 1999). And the major Pleistocene glacial cycles (Berger and Loutre 2004) reveal spectral power in the periods of Earth's precession, obliquity angle, and orbital eccentricity (Hays et al. 1976). What triggers these changes is not yet established. But because they are common to the same Earth system, it is possible that their forcing mechanisms are functionally related. Therefore, it is useful to consider them simultaneously, for a solution in one time scale may inform another. Along these lines, Cane (1998) cites the similarities in tropical convection in ice age and La Niña climates, an idea that is the basis of the 'tropical hypothesis' of glacial forcing (Cane and Clement 1999; Chiang 2009). Here I propose that the tropical hypothesis works through the common mechanism of Pacific countercurrent consolidation (PCC), driven by a combination of tidal and orbital cycles that span interannual, millennial, and orbital time scales.

The leading criticisms of the topical hypothesis in the millennial and orbital domains are the lack of a 'flywheel' that can hold the tropical ocean-atmosphere system in one state or another for centuries or longer (Broecker, 2003), and the lack of a proven abrupt trigger (Clement and Peterson 2008). Here the proposed flywheel is the inherently bi-stable latitudinally asymmetric position of the ITCZ, as modeled by Wang and Wang (1999). Abrupt change follows abrupt shifts in that position, as occurs in the present annual cycle.

In the orbital time scale domain, the leading alternative to the tropical hypothesis is the original Milankovitch model in which glacial terminations are paced by maxima in northern hemisphere summer insolation. To support this interpretation, many studies plot July insolation at 65°N in parallel with variation in global ice volume. However, the timing of July insolation maxima is the same at all latitudes, perihelion being global. So the qualification "at at 65°N" does not itself corroborate the Milankovitch model. For example, the timing of the same curve supports a warm Southern Hemisphere winter narrative (only the amplitude is latitude dependent). Furthermore, abrupt climate discontinuities at glacial terminations occur when July insolation remains as low as during many glacial stages, so it is only the mature phase of interglacials that correspond to July insolation maxima (Denton et al. 2010). What triggers the earlier discontinuity is unresolved. Instead, here I propose that March perihelion determines when the ITCZ jumps north. Cheng et al. (2009) accurately date 'weak monsoon intervals' that mark the four most recent terminations, at 15-17, 129-136, 242-250, and 336-343 thousand years ago (kyr). March perihelions are at 17, 133, 247, and 340 kyr.

Tidal forcing of millennial change is proposed by Keeling and Whorf (1997, 2000), who identify a 1,800 year cycle of "repeat coincidences" of maximum tide raising force that may trigger global cooling through generally increased vertical ocean mixing. Cerveny and Shaffer (2001), Treolar (2002), and Ffield and Gordon (1996) also propose tidal forcing of the ENSO and other ocean-atmosphere dynamics. Munk et al. (2002) confirm the prominence of the 1,800 year tidal cycle of Keeling and Whorf (1997, 2000), but question whether its 0.04 mm amplitude is sufficient to affect global climate. However, in the present hypothesis the tidal signal need only excite an internal gravity wave resonance in the existing shear layer bounding the Equatorial Undercurrent (EUC). In a study of shear turbulence in the EUC, Gregg et al. (1985) conclude, “Mixing in this zone resembles a sharply tuned harmonic oscillator, which can have large output changes for small forcing perturbations.” So here the weak tidal signal first leverages EUC shear energy, and further leverages global ENSO teleconnections.

Section 2 first presents the integrated time scale hypothesis as a whole. Sections 3, 4, and 5 then respectively present evidence of its operation in the interannual, millennial, and orbital time scale domains. Section 6 sumararizes.

2. Integrated hypothesis

The orbital cycles that pace the ices ages did not change 2.75 million years ago when northen hemisphere glaciation began. Therefore, a complete explanation of global climate forcing must first answer what changed at that time. Cane and Molnar (2001) present evidence that coincident closure of the Indonesian Throughflow was determinant. Among several consequences, this closure formed the western barrier necessary to contain the elevated sea surface in the western equatorial Pacific warm pool, which Wyrtki (1985) and Jin (1997a,1997b) show is a necessary condition for ENSO instability. In another hypothesis, Fedorov et al. (2006) link concurent thermocline shoaling to the emergence of the eastern Pacific cold tongue, which is also a necessary condition of ENSO instability. So in support of the tropical hypothesis, cyclical northern hemisphere glaciation began when the stage was set for the ENSO to begin.

2.1 PCC

Figure 1 diagrams the integrated hypothesis, beginning with the proposed short time scale ENSO trigger. This mechanism involves ocean currents dynamics that are not addressed in prevailing ENSO models (Wang and Picaut 2004). The trade wind driven westward South and North Equatorial Currents (SEC and NEC) ‘set up’ the western warm pool sea surface. In response, the primary eastward gradient driven countercurrents include the EUC, which runs below the SEC, and the North and South Equatorial Countercurrents (NECC and SECC). The NECC extends across the Pacific between 5°N and 9°N, but with a usual northern springtme migration to the equator in the west, while the SECC seldom extends past the date line. But Johnson et al. (2002) show the EUC connected to both the NECC and the SECC within the thermocline at 156°E, so at their outset the countercurrents are a continuous ribbon of eastward transport whose edges breach the surface. This ribbon extends from 8°N to 4° S (1,333 km), with a vertical extent of 50 m to 200 m (Fig 2 of Johnson et al., 2002). It shifts slowly north as the SECC fades, while the EUC and NECC are contiguous as far east as 155°W. Friction in the shear layers above and below this ribbon is what restrains the eastward release of gravitational potential. The eastward advection of warm pool surface water at El Niño onset can therefore be understood as an acceleration of that release. I propose that PCC triggers the acceleration by reducing the specific surface area of the ribbon. Initial PCC occurs when NECC transport merges geostrophically into the EUC at El Niño onset (Picaut et al. 1996).

2.2 Interannual and millennial PCC forcing

What can cause PCC? Sverdrup (1947) explains that the extent of the NECC's northward excursion results from a balance between equatorward geostrophic impulse, poleward Ekman impulse, and so-called Sverdrup transport, which is the poleward reaction to vortex stretching by positive wind curl north of the equator. However, the vortex stretching term presumes conservation of vorticty, so a sporadic phenomenon that dissipates that vorticy could cause PCC by weakening net-northward Sverdrup transport. I propose that ITR, or an increase in its frequency, is what does this in interannual and millenial time scales. The ITR examples presented in Section 3 contain semidiurnal temperature variation of up to 9°C, reflecting thermocline heave exceeding 100 m, with maximum excursions coincident with local meridian passage of the sun and moon, and semidiurnal zonal current reversals indicating large scale overturning. In such turmoil, I submit that a water parcel cannot retain a memory of an earlier rotation, as conservation of vorticity requires. Ray (2007) questions whether peak tides can influence climate because they are of short duration. But here, even if sporadic ITR persists for as little as three days, the consequence of lost vorticity is long-lasting.

The sporadic and quickly amplifying character of observed ITR, together with its concentration in the shear layer above the EUC, suggests that it develops from internal gravity waves when the local buoyancy frequency falls within the tidal band. Mechanically, extreme thermocline heave in ITR may dissipate vorticity by forcing vertical motion that rotating bodies resist (by the Taylor-Proudman theorem), resulting in non-linear increases in friction (as rocking a toy gyroscope quickly brings it to rest by increasing its bearing loads). ITR appears qualitatively related to the phenomenon of "Kelvin fronts" theorized by Fedorov and Melville (2000).

Two modeling studies support the above mechanism. First, by isolating advection and friction effects, Kessler et al. (2003) deduce unexplained friction concentrated between 2°N and 2°S, which would tend to reduce positive relative vorticity along the EUC. Also, their model does not reproduce observed eastward transport at 3°N to 6°N west of the date line, and places the NECC farther north in the western Pacific than Johnson et al. (2002) observe. Second, Brown and Fedorov (2010) conclude that the classical presumption of linear friction-free Sverdrup balance is not consistent with observation. And their model simulates a western EUC with up to 50% less transport than Johnson et al. (2002) observe, which could reflect overestimated Sverdrup transport out of the equatorial box. Both models deduce an unknown source of friction, and simulate countercurrents that are overly diverged, consitent with the proposed ITR-PCC dynamic.

2.3 Orbital time scale PCC forcing

Figure 1 next indicates the mutual PCC forcing by the combination of September to March perihelion and obliquity angle < 23.5°, that shifts the ITCZ to its southern stable position on the equator. The NECC then simply follows the the ITCZ equatorward, per Sverdup (1947), resulting in PCC. Note that the original motivation of Harold Sverdrup's anaysis was to understand why the NECC follows the ITCZ. Global cold phases correspond with southward ITCZ displacements in both millennial and orbital time scales (Haug et al 2001; Koutavas and Lynch-Stieglitz (2005); Wang et al. 2004).

With respect to the precessional influence, September to March perihelion (in southern summer) is when the cross equator temperature gradient tends to draw the ITCZ south, and vice-versa during March to September perihelion. These transitions are abrupt because insolation contrast on the equator is greatest at the equinoxes (Kukla et al. 2002; Kukla and Gavin 2004). However, equatorward ITCZ migration also requires low obliquity, when the northen hemisphere is not preferentially warmed by longer summers (Huybers 2006), and vice-versa when obliquity is low. This is the basis of mutual precession-obliquity control discussed in Section 5. Raymo and Nisancioglu (2003) and Kukla and Gavin (2005) also link global cooling to the cross-equator temperature gradient, but towards bulk poleward heat and moisture transport rather than as an ITCZ switch.

The Huybers (2006) northen summer obliquity control may be complimented by a tidal effect, as indicted by the dashed line in Figure 1. The prominence of low latitude equinoctial tides indicates strong declination dependence, so lower obliquity angle must strengthen low latitude tides, by in effect being 'more equinoctial' all year. This would strengthen ITR forcing when obliquity angle is low, and further contribute to cold phase PCC.

The proposed March and September transitions are also aided by interaction with the annual cycle in the tropical Pacific. While equinoctial insolation is equatorially symmetric, the annual cross equator trade wind cycle is not (Clement et al. 1999, 2000, 2001; Kukla and Gavin 2004, 2005). The equatorial Pacific adopts the seasonal cycle of the non-ITCZ southern hemisphere (Wang and Wang 1999), which is warmest in March and coldest in September. Therefore September perihelion weakens the annual cycle, which weakens southeast trade winds in the eastern Pacific, and further supports the equatorial ITCZ position. In a cross-time scale interaction, a weak annual cycle also inceases ENSO frequency, and vice-versa (Timmermann et al. 2007a; Chiang et al. 2008; Fang et al.

2008). Here the proposition that cold periods have high ENSO activity of both types differs from the Clement et al. (1999) experiment which defines warm phases as high El Niño frequency. Their model restricts ITCZ migration, so does not address the dynamic proposed here.

2.4 ESLN formation

Triggered by the above means, PCC is proposed to be common to global Quaternary cooling in all its frequencies. When the warm pool sea surface is elevated, the initial result of PCC is a transient El Niño event. Subsequently, if ITR persists or the ITCZ becomes orbitally locked in its equatorial position, PCC then forces an equatorially symmetric La Niña (ESLN) mode, distinguished from other La Niña by an equatorial "cold eye" centered near 140°W, with warmer sea surface temperature farther east. In the instrument record, ESLN occurred in June-August 1998, following termination of the 1997 El Niño. For context, Figure 2a plots July 1996 surface current showing the usual NECC position trending northward per Sverdrup (1947). Figure 2b then shows the initial warm pool advection PCC in July 1997, and Figure 2c shows the subsequent cold phase PCC surface jet near 140°W in July 1998, with the NECC conspicuously absent. Figures 2d and 2e plot the corresponding sea surface temperature and chlorophyll anomalies.

Murray et al. (2000a, 2000b) provide proxy records of peak carbonate sedimentation rates at glacial onset along 140°W. The meridional distribution of these sediments is similar to that of the record-setting 1998 plankton bloom (Chavez 1999) shown in Figure 2e, which provides evidence of glacial ESLN. Lyle et al. (1992), Pedersen (1983), Paytan et al. (1996), and Beaufort et al. (2001) also observe increased glacial sediment accumulation rates in the equatorial Pacific. Because the EUC contains iron (Ryan et al. 2002; Wells et al. 1999), the 1998 ESLN may be regarded as Earth's largest natural iron fertilization experiment (Coale et al. 1996).

The structure of the mid-Pacific tidal amphidrome provides an explanation for why ESLN's distinguishing cold eye is centered at 140°W. In the dominant M2 constituent, one of two centers of maximum amplitude is on the equator between 145°W and 135°W (Lyard et al. 2006). In a momentum balance of the 1997-1998 event, Grodsky and Carton (2001) conclude that local acceleration, zonal pressure gradient anomaly, and wind induced momentum flux were uncorrelated between 140° and 120°W in May 1998. They attribute this to non-linear vertical advection and mixing processes, consistent with locally strengthened tidal dissipation. In turn, this would strengthen PCC in that zone, which accordingly is where Johnson et al. (2002) and Kessler et al. (2003) observe maximum mean EUC transport.

Jones (1973) describes the process by which EUC shear energy converts to potential energy in the underlying pycnostad, or "thermostad" or "13°C water" (in the sense that the center of gravity of a mixed water column is higher than if stratified). Increased shear associated with consolidated eastward transport would thereby thicken the pycnostad locally, which in turn would elevate the overlying thermocline locally. Figure 2f shows the 12°C isotherm rising to a depth of 240 m during May-December 1998.

Two self reinforcing feedbacks act to maintain ESLN once it is established. First, the thermocline ridge that otherwise defines the NECC's northern boundary (Wyrtki and Kilonsky 1984) is absent, as also occurred in the second year of the 1982-1983 ENSO cycle (Meyers and Donguy 1984). This facilitates upwelling within the cold eye by removing the barrier to northern source pycnocline water. Second, the winter monsoon cell that forms over the cold eye generates meridionally diverging surface winds that further strengthen upwelling that powers the winter monsoon cell, etc. Speculatively, if the above pycnostad thickening brought the pycnostad to the surface, at some water column temperature higher than the present pycnostad, this heat engine feedback would accelerate with transformative consequences.

Pacific Hadley cell division by the cold eye winter monsoon cell is a de facto ITCZ shift to the equator, as indicated by the upwards arrow in Figure 1. By this means, the ITR-PCC-ESLN dynamic forces southward ITCZ migration in interannual and millennial time scales. This occurred both in 1998 and in the second year of the 1982-1983 ENSO cycle (Vecchi 2006). Accordingly, Sachs et al. (2009) show that the mid-Pacific ITCZ was shifted south by up to 500 km during the Little Ice Age, when Gergis and Fowler (2009) observe high La Niña frequency.

2.5 ESLN teleconnections

In the first of five possible global cooling effects of ESLN, the winter monsoon cell weakens the divided rising branch of the the Hadley circulation by exchange of latent heat, which reduces the supply of tropospheric water vapor, the dominant greenhouse gas. This provides the mechanism of glacial tropical water vapor reduction that Broecker (1997) and Seager et al. (2000) require, and is consistent with the Cane (1998) and Cane and Clement (1999) description of cold phase climate. Subsidence within the winter monsoon cell would also oppose the small but critical transfer of water vapor to the stratosphere (Solomon et al. 2010). Oort and Yienger (1996) found an inverse relationship between Hadley circulation strength and La Niña events that supports this ESLN effect.

Second, a weaker Pacific Hadley cell also draws the subtropical subsidence zones equatorward, the oposite of what Seidel et al. (2008) observe in recent dacades. Globally, this constriction of the tropical belt narrows the area of planetary heat gain, and reciprocally expands the poleward areas of planetary heat loss.

The third result of a cold phase La Niña regime is a poleward shift of Northern Hemisphere storm tracks (Seager et al. 2009). This may increase precipitation in the Canadian Maritimes, via the shorter great circle course from the Gulf of Alaska to Baffin Bay. While maritime glaciers presently surge in response to warming, increased iceberg production during cold Heinrich events (Heming 2004) requires increased mass to increase pressure mediated basal melting. So a poleward displacement of North Pacific storm tracks could deliver the required precipitation. And the northern Rocky Mountains allow easier zonal transport (Seager et al. 2002) because they are lower in altitude. Wunsch (2010) questions whether melting drift ice alone can distribute sufficient fresh water to shutdown North Atlantic overturning, as is observed. An ESLN enhanced precipitation source, if only in summer, could satisfy this requirement. An increase in fresh water supply to the North Atlantic would also expand winter sea ice. Such reorganization is suggested by Steffensen at al. (2008), who observe warmer marine moisture sources during cold phases in North Greenland deuterium excess.

The fourth ESLN effect is the teleconnections between ENSO and the Antarctic Dipole. Yuan et al. (2004) show that its La Niña mode causes (a) full development of the southern branch of the split South Pacific jet stream (polar front jet), so that its connection with the single jet in the Atlantic sector forms a complete circumpolar jet; (b) a decrease in poleward heat flux into the Pacific sector; (c) an increase in storms in the Pacific sector; and (d) an increase in sea ice cover in all sectors except the Weddell Sea (at 40°W), resulting in a net increase in southern hemisphere sea ice cover. This is a fast response, for Hanna (2001) records a 2.2 standard deviation increase in Pacific sector sea ice in September 1998, which he attributes to ENSO. While the opposing El Niño mode is a mirror image in the Atlantic sector, persistent ESLN would compound the net positive sea ice expansion, leading to a positive southern hemisphere ice-albedo feedback. Interestingly, Schlosser et al. (2011) find a possible warm bias in Antarctic ice cores due to seasonal warm air intrusions from ice edge cyclogenesis, as may result from the cold phase Antarctic Dipole storm influence. This may be relevant to present understanding of the bi-polar see-saw dynamic.

A speculative final global ESLN effect is on CO_2 efflux from the central and eastern equatorial Pacific, which is presently the largest oceanic source area (Takahashi et al. 2002). As CO_2 is fungible in the atmosphere, a reduction in this source is equivalent to a sink elsewhere. Increased export production at glacial onset (Murray et al. 2000a, 2000b), as modeled by the 1998 bloom (Chavez 1999), must have utilized a portion of this CO_2 prior to efflux. But this result would be offset by increased upwelling of CO_2 rich pycnocline water.

ESLN structure may resolve two apparent contradictions in proxy records. First, the separation of the ESLN cold eye from the South American coast may explain conflicting sea surface temperature proxies in the far eastern Pacific. Whereas Cane (1998) associates La Niña with global cooling, Koutavas at al. (2002) conclude that higher stadial sea surface temperature near the Galapagos indicates El Niño, as Ortiz at al. (2004) also observe at a site near the southern tip of the Baja Peninsula. However, the core locations used in these studies are within the Fig 2(e) warm anomalies in the far eastern Pacific during the 1998 ESLN. Second, ESLN may explain high stadial sea surface salinity in the western warm pool region, which Stott et al. (2002) attribute to the modern El Niño pattern in which deep convection migrates eastward. If glacial ESLN were persistent, westward SEC surface transport would be more saline due to increased evaporation by dry subsiding air in the winter monsoon cell.

3. Interannual manifestation

Figure 3 presents a first example of ITR at 0°N 165°E at the spring onset of the 1997 El Niño. Vertical lines indicate tide maxima at new (N) and full (F) moons, and solar (S) and lunar (L) eclipses. A leading instance of ITR is the 14 to 24 February detail view (f, g), in which vertical lines indicate local meridian passage of the moon (blue) and sun (red). A resonance at 150 m drives semidiurnal temperature spikes of up to 8°C (g), coincident with local meridian passage of both the sun and moon beginning in quadrature. The corresponding one hour resolution zonal currents (f) at 100 m (solid green) and 150 m (dashed green) are anti-correlated with each other, with semidiurnal reversals, indicating tidally paced overturning in the thermocline. Another example at 4 to 14 March (h, i) shows semidiurnal temperature (i) resonance at 175 m. Anti-correlation of 100 m zonal (green) and meridional (red) currents (h) indicate semidiurnal southwestward tidal pumping. The context of these ITR examples is as follows: A latitude-time plot (Figure 3a) of 5 day average zonal wind anomaly along 165°E shows a westerly wind burst (WWB) centered on the solar eclipse of 9 March; tide height (b) at the Marshall Islands (8.7°N 167.7°E) shows the corresponding tide maximum, with reduced semidiurnal inequality at the equinox; geocentric lunar distance (c) relates perigee to tidal variation, which is highest at the March 9 perigean eclipse; daily subsurface zonal (green) and meridional (red) currents (d), averaged over 30-245 m with 20°C isotherm depth (blue, scale on right), indicate a distinct peak in southward transport two days after the 9 March eclipse, and other southward excursions are near other tidal maxima. One hour resolution temperatures (e) at nine depths are distinguished by the color key shown. The above data spans the formation of the second of two downwelling Kelvin waves known to initiate the record-setting 1997 El Niño (McPhaden 1999), shown here to have formed in a dissipative context with distinct southward transport at peak tides. Note that ITR beginning 16 February precedes the WWB centered on the 9 March eclipse.

Figure 4 similarly details a second ITR episode at 0° 165°E during the start of the 2002 El Niño (McPhaden 2004). The 7 to 22 November 2001 detail view (f) indicates semidiurnal resonance at 150 m, and ITR amplitude in December reached 9°C within 12 hours. Here the context is a solar eclipse on 14 December 2001 coincident with another WWB (a) and another southward (red) pulse of average subsurface current and a maximum downward 20°C isotherm excursion (d) on the same day as the eclipse. This acute example is relevant to differentiating WWB and ITR effects, as both eastward and southward subsurface acceleration is simultaneous at all depths to 150 m on the day of the eclipse, but is strongest at 110 m zonally and at 130 m meridionally. In contrast, wind forcing alone would be strongest at the surface and propagate downward. The WWB peaks at 11.4 m/s one day after the eclipse. And as in Figure 3, note that ITR during 11 to 20 November precedes the WWB. Also note that the tidal range in December 2001 (Figure 4b) is less than near the equinox in March 1997 (Figure 3b).

In the western equatorial Pacific mean tidal transport is southward, in counterclockwise rotation about the mid-Pacific amphidrome (Lyard et al. 2006). This is apparent in both Figures 3 and 4, where pulses of southward subsurface current coincident with peak tides. This raises a question, whether the steep equatorial thermocline ridge functions as a bathymetric feature in internal tide generation (Garrett and Kunze 2007). Or does the southward upward sloping thermocline merely accelerate southward transport, like a beach? In either case, sudden tidal advection of warm surface water to the equator could play a role in initiating downwelling Kelvin waves.

Provided these two examples of ITR, Figure 5 contrasts the weekly 1993-2007 Niño 3.4 index (a) with a latitude-time surface current plot along 165°E (b) that shows PCC at El Niño onset (Picaut et al. 1996). Vertical gridlines are at the March equinox. A wavelet analysis (Potter reference) of subsurface temperatures at 150 m (c) shows elevated spectral power in the 12 hour semidiurnal tide band prior to El Niño onset in 1997, 2002, and 2006. Note that semidiurnal power at 150 m drops out during 7 to 21 March when Figure 3 shows ITR shifted to 175 m depth. Semidiurnal power also precedes an upturn in the Niño 3.4 index in early 1999, and following an extreme central eclipse in July 2000 discussed below. Next, to relate the above interannual variation to potential tidal forcing cycles, Figure 5d shows the time distribution of eclipse seasons. Graphically, eclipses are shown in groups of 2 or 3 one fortnight apart, projecting downards in decreasing absolute value of gamma. Gamma is the measure of eclipse centrality, equal to the moon's closest approach to the axis of the sun-Earth shadow cone in Earth radii (ER) (NASA). Figure 5e is geocentric lunar distance, showing both the mean 27.55 day anomalistic month (perigee to perigee), and the secondary cycle in lunar "proxigee", or close perigee (Wood 1986) that repeats every 7 or 8 anomalist months, with a mean repeat period of 207 days as discussed below. Figure 5f is a western Pacific tidal energy measure in the daily sum of vertical tide displacements at the Marshall Islands. These sums reflect both amplitude maxima and reduced diurnal inequality at the equinox (Wood 1986), but ENSO related changes in sea level (Wyrtki 1985) cancel. There are generally four differences per day between higher high water (HHL), low water (LW), high water (HW), and lower low water (LLW); in the rare cases of 3 or 5, the daily sum is multiplied by 4/3 or 4/5 respectively, which does not alter the form of the curve.

There is a clear equinoctial concentration of low latitude tidal power. The peak daily value shown is lunar proxigee on 28 March 1998, with other maxima in 2002 and 2006.

The above instrument records show examples of ITR that emerge prior to WWB forcing, so the ITR phenomenon cannot be a tidal amplification of wind stress energy. Also, its uniquely tidal semidiurnal frequency means it cannot be the result of other equatorial wave interactions. The ocurrance of ITR prior to upturns in the Niño 3.4 index therefore strongly suggests a causative role, consistent with PCC mediated ENSO. In operation, I propose that tidal power near the vernal equinox has the greatest climate impact because that is the season of weak trade winds, weak ITCZ bias, and the NECC's annual migration to the equator in the western Pacific. This is when these elements are in a state of flux, and therefore most suseptable to exterrnal forcing. So uncertainty in the the well known spring predictability barrier in ENSO forcasting may be resolved by knowing how strong the tides are.

Two overlapping cycles are proposed to explain the observed maxima in Marshall Islands tide displacement in 1998, 2002, and 2006. First, the eclipse seasons repeat in the 9 year plus 5 day half Saros eclipse cycle, discussed below, which approaches the vernal equinox in 1997 and 2006 (Figure 5d). Secondly, the proxigee cycle approaches the vernal equinox in 1997, 2002, and 2006. Taken together, these cycles coincide with El Niño onset in 1997, 2002, and 2006. Note that tidal forcing is strong in both 1997 and 1998, which explains the persistence of PCC after the initial warm water discharch, eventually leading to ESLN in the summer of 1998.

Another circumstance of stong tidal forcing is related to extreme central eclipses, as noted above preceding ITR in July 2000. These low gamma eclipses (LGE) are the basis for the millennial cycle described below, but are also evident in the instument record. In the 1871-2010 Multivariate Enso Index (MEI), LGE's coincide with the onset of warm events in 1877, 1888, 1902, 1940, 1951, 1982, 1991, 2002, and 2009. And the LGE in July 2000 ocurred when the warm pool was discharged, so its effect was to delay recharge (and thereby prolong the subsequent cold phase).

Taken together, at least one circumstance of LGE, vernal eclipse, or vernal proxigee forcing (using a +/- 30 day window from 21 March) is present in 79 of 140 years in the MEI domain, and coincides with 19 of 22 warm events. But a full accounting of tidal causation must control for forcing overlap and available warm water volume, as in 1997-2000.

4. Millennial manifestation

Proposed tidal forcing in the millennial domain is through a 586 year cycle in the frequency of LGE's. Their proposed physical significance is not their individual passing power, but rather in how they perturb the lunar orbit. Their impact is not restricted to vernal equinox.

For background, eclipse periodicity follows the 9 year plus 5 day half Saros cycle of alternating solar and lunar eclipses known in Baylonian times (Steves 1998), which is distinct from the 18.6 year nodical cycle. Individual Saros series may exceed 1,400 years, and the gamma values of their eclipses converge to zero (most central) at their midpoints. By convention, an eclipse is a sysygy with absolute value of gamma < 1.6 (NASA). At any given time, approximately 58 overlapping solar and lunar Saros series progress through the 5 to 6 month eclipse cycle, but their collective degree of centrality varies over time. The midpoints of successive Saros series are separated by the 29 year less 20 day INEX interval of van den Burgh (1955).

The Saros is equal to 223 synodic months (mean S = 29.530589 days new moon to new moon or full moon to full moon) and 242 Draconic months (mean D = 27.21222 days node to node when the moon crosses the ecliptic). The S-D beat period, 1/((1/D)-(1/S)), is the 346 day eclipse year (11.73766S =12.73766D), 19 of which approach the Saros at 223S≈242D. The INEX equals 358S. Each eclipse year contains two eclipse cycles, when each of the moon's nodes face the sun. 242 being even, the half Saros is 111.5S, which alternates solar and lunar eclipses in 19 eclipse cycles. Due to planetary resonance (Steves 1998), the Saros is 239 anomalistic months (mean A = 27.554551 days perigee to perigee). The S-A beat period (13.94434S = 14.94434A) is 411.78 days, 8 of which approach the half Saros. The S-A beat also approaches the 413.37 day evection period at 14S≈15A. At the ends and near the middle of each evection period there is a mutual 3-body attraction in space that draws the moon closer to earth at proxigee, as shown in Figure 5e, yielding 2 proxigee cycles of 7S each. But as 15A is odd, the coresponding number of anomalistic months cannot divide in half evenly, so the mean 207 day proxigee cycle is 7S and either 7A or 8A, causing a mutual perturbation of S and A in which the advance of lunar perigee in longitude actually reverses direction (Wood 1986). In this perturbation, the length of the 27.55 day anomalistic months varies by up to 3.9 days, while the complimentary synodic month variation is up to 0.5 days. The significance of this perturbation is that decreasing S with increasing A results in 5 month long spans of reduced perigee-sysygy intervals (PSI) (Wood 1986). This means that the tide raising effects of perigee and sysygy are drawn closer together for a period of 5 months.

A first attribute of LGE‘s, with absolute value of gamma below approximately 0.25, is that lunations a fortnight before and after are also eclipses, forming a triple as centered on 22 August 1998 and 16 July 2000 in Fig. 5d. This concentrates tidal forcing because the moon is closer to the plane of the ecliptic at each of these three lunations. Secondly, if a member of such a triple occurs within 24 hours of perigee, it is proxigee, due to the above S-D-A perturbation. The degree to which LGE's attracts proxigee is indicated by comparison of lunar distance. In the 100 year period 1911-2010 there are 456 eclipses, at which the average geocentric lunar distance is 380,746 km. 35 of these are LGE's, at which the average geocentric lunar distance is 362,862 km, a 4.7 % reduction (MICA). Lastly, the LGE's that are at proxigee center the above 5 month long spans of reduced PSI.

Figure 6a plots the number of LGE events per 50 years for 5 kyr in the late Holocene. Maxima in the 586 year LGE frequency cycle correspond with the Little Ice Age and Bond cycles #1 and #3 in Icelandic glass (Bond et al. 1999). An intermediate LGE peak coincides with the 1150 drought in the Americas (Cook et al. 2004). The Steffensen et al. (2008) study shows 400-650 year centennial cycles within millennial cycles. High LGE frequency during the Little Ice Age is consistent with high La Niña frequency (Gergis and Fowler 2009) and southward ITCZ migration (Sachs et al. 2009) noted above.

Figure 6b is the day-year plot that coresponds with Figure 6a. Red diamonds and blue circles respectively represent lunar/solar/lunar (L/S/L) and solar/lunar/solr (S/L/S) triples, so upward rightward sloping blue-red series indicate the half Saros advance of 5 days per 9 years. Placement of yellow squares indicate LGE'a at proxigee. The INEX slope regresses 20 days per 29 years, drawn through the 16 July 2000 LGE. This figure is the Saros-Inex Panorama of van den Bergh (1955) plotted in time, but only showing the most central eclipses, which are LGE's. Van den Bergh (1955) provides an astronomical measure of the LGE distribution in the 586 year Tetradia cycle in repeating lunar tetrads (four successive total lunar eclipses).

A wave form that reflects a variation in the rate of change of gamma deviates from the INEX in a way that yields the variation in LGE frequency in Figure 6a. In individual half-Saros series, the rate of change of gamma accelerates as their 5 day steps advance towards aphelion (and vice-versa towards perihelion). This results from "stern chase" variation in the length of the synodic month, a term of nineteenth century celestial navigation referring to the time the moon requires to catch-up with Earth at sysygy. Accordingly, between 1800 and 2050, synodic months ending in July (near present aphelion) are an average of 4.07 hours shorter than those ending in January (near present perihelion) (MICA). This is significant relative to the above 0.5 day perturbation in S. So as Earth slows at aphelion (by Kepler), the stern chase becomes shorter, which shortens S, so the progression to commensurability with D accelerates with respect to the INEX. Sucessive wave forms then precess with aphelion, and their relationship reflects the fact that 10 Inex = 16 Saros + 12S, as all eclipses have neighbors 12S ahead and 12S behind whose Saros series numbers differ by 10 Inex steps. The wave to wave transition is a 12S phase shift.

Because of the stern chase dynamic, a reduction in earth eccentricity would straighten the wave form towards the INEX line, which would reduce contrast in the 586 year cycle, and thereby dampen resulting millenial time scale climate cycles. However, an increase in present eccentricity may also dampent millennial change, because a more acute wave form would align low LGE frequency before aphelion with high LGE frequency after aphelion.

The relation of perigee to LGE's is governed by the anomalistic month's commensurability with the 358S INEX interval. 358S is incommensurate with A, leaving a remainder of 0.673. The first close fit is therefore at 3 INEX = 1074S = 1151.02A = 86.83 years, so proxigee is concentrated at every third Saros series in Figure 6b. This period is reflected in the spectral analysis of Treolar (2002), who correlates tidal maxima with high (cold phase) SOI in 86.795, 20.295, and 18.02 year (the Saros) “mid-latitude” cycles. Higher S-A commensurabilities are at 15,283S ≈ 16,279A = 1,237 years, 20,805S ≈ 22,297A = 1,682 years, and 22,548S ≈ 24,165A = 1,823 years, which relates to the Keeling and Whorf (1997, 2000) 1,800 year period. Of these, 1,237 and 1,823 are near 2x and 3x multiples of 586. On this basis, the last proposed tidal forcing cycle incorporates proxigee, at 2x or 3x multiples of the 586 year LGE cycle, equal to 1,172 and 1,758 years. Bond et al. (1999) observe cold phase periods in a range between 1,328 and 1,795 years that average 1476 +/- 585 years, corresponding to the 1,470 year Greenland Ice Sheet Project 2 spectral peak (Grootes and Stuvier 1997). However, the nearby Greenland Ice Core Project record shows separate peaks at 1,163 and 1,613 years (Hinnov et al. 2002), and a Sulu cave record yields separate peaks at 1,190 and 1,667 years (Clemens 2005).

5. Orbital manifestation

By the orbital time scale mechanisms described in Section 2.3, dual control by the 19-23 kry precession cycle and the 41 kry obliquity cycle is according to this rule: (a) glacial termination occurs at conjunctions of March perihelion and rising obliquity > 23.5°; (b) the fast melt portion of interglacial periods ends 10 kry later; (c) if obliquity > 23.5°, then interglacial continues; and (d) glaciation begins after September perihelion and before March perihelion when obliquity < 23.5°. So precession paces abrupt terminations, obiquity can extend the length of interglacials, and control of which cycles are skipped is mutual.

Figure 7 illustrates the manifestation of the above rule over the past 3 million years (myr): (a) March insolation at the equator (Berger 1978; Laskar et al. 2004); (b) the LRO4 δ^{18}O ice proxy stack (Lisiecki and Raymo 2005); and (c) obliquity angle (Berger 1991). Half precession cycles between March and September perihelion are highlighted in red, and intervals of obliquity > 23.5° are highlighted in green. Note that there are both anomalously long and short half precession intervals when eccentricity (precession amplitude) is low (Berger 2003), and the duration of high obliquity decreases with obliquity amplitude. Uncertainty in the LR04 stack is 4 kyr since 1 myr, and 6 kyr from 3 to 1 myr, with orbital tuning to obliquity (Lisiecki and Raymo 2005).

First with respect to the precession cycle, as Berger (1978) observes in the most recent instance, intervals of fast ice melt exceeding 0.50 ‰ dO^{18} begin near March perihelion and end near September perihelion in 17 of 17 cases since 1 myr, in 17 of 20 cases between 1 and 2 myr (exceptions are MIS 34, 36, and 42), and with weaker correspondence earlier. These 10 kyr fast melt intervals, shaded darker red in Figure 7, are common to both 40 kry and 100 kyr glaciations, which explains the apparent increase in ice age skewness with amplitude (Broecker and van Donk 1970; Lisiecki and Raymo 2007).

The 10 kyr half precession fast melt interval further explains why glacial cycles must skip precession cycles. Ice sheets accumulate slower than they melt, so there is not enough time in the cold half to freeze an equal volume if ice. Exception to this rule would result in stepwise cycles leading to no ice.

With respect to obliquity, Huybers and Wunsch (2005) and Huybers (2007) establish that high obliquity is a necessary condition of glacial termination, based on statistical analysis of a successful three parameter model that adopts the 10 kry ice volume reset interval of Marshall and Clark (2002). Huybers (2006) attributes this forcing to the extended duration of northern high latitude summers. But the Marshall and Clark (2002) reset interval is also the above half precessional interval. Huybers (2007) shows that the transition to longer cycles is due to skipped obliquity cycles, but what determines which ones are skipped is not established (Liu et al. 2008) or considered chaotic (Huybers 2009). But note in Figure 7 that skipped obliquity cycles are the ones with the poorest alignment with March perihelion (at 50, 100,175, 380, 460, and 660 kyr).

Mutual precession-obliquity control explains the mid-Pleistocene transition, for this is when the phase relation between precession and obliquity changed from 1:2 (40 kyr period), reflecting the Berger and Loutre (2004) “high-low-high” dynamic in obliquity/precession conjunctions, to 2:5 or 3:5 (80 or 120 kyr period), as Ruddiman (2006) observes. The period of precession is not constant (Berger et al. 2003). This interdependence reconciles proposed forcing by quantized precession (Raymo 1997) and quantized obliquity (Huybers 2007).

In parts (c) and (d) of the proposed orbital forcing rule, obliquity > 23.5° determines whether interglacial periods continue after September perihelion, when the slope of the LR04 stack levels off, as at present and at MIS 7, 11, 13, 17, 37 and 47. By this rule, glacial onset following the Holocene 6050 kyr altithermal at September perihelion (Kukla and Gavin 2004) was forestalled by 24.1° obliquity. This provides an opportunity to access the integrated hypothesis when ENSO proxies are available. After 5,790 +/- 90 years ago, Sandweiss et al. (1996) observe a transition to temperate Peruvian mollusk assemblages compatible with ENSO variability. After 5,400 ka, Haug et al. (2001) observe a trend towards dry conditions in the Cariaco Basin, with a southward ITCZ shift. These proxies are consistent with the present hypothesis, by which north ITCZ bias weakens after September perihelion, which also leads to higher frequency PCC-ESLN cooling.

Perihelion is now in early January and obliquity is 23.446°, and at the next March perihelion 4 kyr in the future it will be approximately 23.0°. Since 1 myr there are 46 January perihelions, of which 6 coincide with declining obliquity between 23.446° and 23.0°, as at present. These are indicated by solid vertical lines above the LR04 stack in Figure 7. All are glacial or at glacial onset, most recently at MIS 9. Earlier exceptions are at 1,686 ka (MIS 59) at low eccentricity analogous to the present (Berger et al. 2003), and the other is at 2,784 ka (MIS G8).

6. Summary

I present a hypothesis that PCC is the common mechanism of global cooling in interannual, millennial, and orbital time scales, consistent with a common Earth system context. An observation of ITR in the western Pacific thermocline prior to El Niño onset informs a novel mechanism of ENSO forcing, whereby ITR leads to PCC by dissipating the vorticity that powers northward Sverdrup transport. PCC alternately results from southward ITCZ migration mutually controlled by precession and obliquity. When persistent, PCC triggers an ESLN mode with these global teleconnections: (a) reduced low latitude tropospheric water vapor; (b) narrowed global mean zone of planetary heat gain; (c) poleward shifted North Pacific storm tracts, that increases North Atlantic precipitation prior to Heinrich events; (d) increased in Antarctic sea ice, by the Antarctic Dipole mechanism; and (e) increased equatorial Pacific export production, that reduces CO2 efflux.

In the interannual time scale, proposed vernal eclipse and vernal proxigee cycles hindcast El Niño onset in 1997, 2002, and 2006. When including LGE events, proposed tidal forcing coincides with 19 of 22 MEI warm events since 1871, where such forcing is present in 79 of 140 years. But a full accounting of tidal causation must control for forcing overlap and available warm water volume, as in 1997-2000.

In the millennial domain, a 586 year cycle in the frequency of LGE's coincides with the Little Ice Age and Bond events #1 and #3. 2x and 3x multiples of the 586 year cycles are consistent with dual spectral peaks in millennial proxies (Hinnov et al. 2002; Clemens 2005).

In the orbital domain, a rule of ITCZ migration under mutual precession-obliquity control is consistent with ice volume proxies, and resolves skewness in glacial cycles and the mid-Pleistocene transition. Global cooling after the 6,050 kyr Holocene altithermal (Kukla and Gavin 2004) is therefore a latent glaciation delayed by high obliquity.

Acknowledgement I thank André Berger for customizing a table of latitude and month specific insolation values which began this inquiry, Dan Potter for assitance in wavelet analysis, Mitch Berkson for assiance in data prepartaion, and early discussions with Irving Sheldon, Jr.

References

Beaufort, L., de Garidel-Thoron, T., Mix, A.C., and Pisias, N.: ENSO-like forcing on oceanic primary production during the Late Pleistocene, Science, 293, 2440-2444, 2001.

Berger, A.: Long-Term Variations of Daily Insolation and Quaternary Climate Changes, J. Atmos. Sci., 35, 2362-2367, 1978.

Berger A. and Loutre, M. F.: Insolation values for the climate of the last 10 million of years, Quat. Sci. Rev., 10(4), 297-317, 1991.

Berger, A. L., Loutre, M. F., and Crucifix, M.: The Earth's climate in the next hundred thousand years (100 kyr), Surveys in Geophysics, 24, 117-138, 2003.

Berger, A. L., and Loutre, M. F.: Astonomical theory of climate change, J. Phys. IV France, 121, 1-35. (doi:10.1051/jp4:2004121001), 2004.

Bond, G. C., Showers, W.,Elliot, M.,Evans, M., Lotti, R., Hajdas, I., Bonani, G., ans Johnson, S.: The north Atlantic's 1-2 kyr climate rhythm: Relation to Heinrich Events, Dansgaard/Oeschger cycles and the Little Ice Age, Geophysical Monograph 112, American Geophysical Union, 35-58, 1999.

Bonjean F. and Lagerloef, G. S. E.: Diagnostic Model and Analysis of the Surface Currents in the Tropical Pacific Ocean, Journal of Physical Oceanography, Vol. 32, No. 10, pages 2938-2954, 2002.

Broecker, W. S.: Mountain Glaciers: Recorders of Atmospheric Water Vapor Content? Global Biogeochem. Cycles, 11(4), 589-597, 1997.

Broecker, W. S.: Does the Trigger for Abrupt Climate Change Reside in the Ocean or in the Atmosphere?, Science, 300, 1519-1522, 2003.

Broecker, W.S. and van Donk, J.: Insolation changes, ice volumes, and the O18 record in deep sea cores, Reviews of Geophysics and Space Physics, 8(1), 169-198, 1970.

Brown, J. M. and Fedorov, A. V.: Estimating the diapycnal transport contribution to warm water volume variations in the tropical Pacific, J. Climate, 23, 221-237, 2010.

Bunn, A.G.: Statistical and visual crossdating in R using the dplR library, Dendrochronologia 28: 251-258, 2010.

Cane, M. A.: Climate change: A role for the tropical Pacific, Science, 282, 59-61, 1998.

Cane, M. A. and Clement, A.: A role for the tropical Pacific coupled ocean-atmosphere system on Milankovitch and millennial time scales. Part II: Global impacts, Geophysical Monograph 112, American Geophysical Union, 373-383, 1999.

Cane, M. A. and Molnar , P.: Closing of the Indonesian seaway as a precursor to east African aridification around 3-4 million years ago, Nature, 411, 157-162, 2001.

Cervany, R. S. and Shaffer, J. A.: The moon and El Niño, Geophys. Res. Letters, 28(1), 25-28, 2001.

Chaves, F. P., Strutton, P. G., Friederich, G. E., Feely, R. A., Feldman, G. C., Foley, D. G., and McPhaden, M. J.: Biological and chemical response of the equatorial Pacific Ocean to the 1997-98 El Niño, Science, 286, 2126-2131,1999.

Cheng, H. C., Edwards, R. L., Broecker, W. S., Denton, G. H., Kong, X., Wang, Y., Zhang, R., and Wang, X.: Ice age terminations, Science, 326, 248-252, 2009.

Chiang, J. C. H.: The tropics in paleoclimate, Annu. Rev. Earth Planet. Sci., 37, 263–97, 2009.

Chiang, J. C. H., Fang, Y., and Chang, P.: Interhemispheric thermal gradient and tropical Pacific climate, Geophys. Res. Lett., 35, L14704, doi:10.1029/2008GL034166, 2008.

Clark, P. U., Webb, R. S., and Keigwin, L. D., eds.: Mechanisms of global climate change at millennial time scales, Geophysical Monograph 112, American Geophysical Union, 1999.

Clemens, S. C.: Millennial-band climate spectrum resolved and linked to centennial-scale solar cycles, Quaternary Science Reviews, 24, 521–531, 2005.

Clement, A. C., and Peterson, L. C.: Mechanisms of abrupt climate change of the last glacial period, Rev. Geophys.,46, RG4002, doi:10.1029/2006RG000204, 2008.

Clement, A., Seager, R., and Cane, M. A.: Orbital control on the El Niño/Southern Oscillation and the tropical climate, Paleoceanography, 14, 441-456, 1999.

Clement, A., Cane, M. A. and Seager, R.: Suppression of El Niño during the mid-Holocene by changes in the Earth's orbit. Paleoceanography, 15(6), 731-737, 2000.

Clement, A., Cane, M. A. and Seager, R.: An Orbitally Driven Tropical Source for Abrupt Climate Change, J. Climate, 14(11), 2369-2375, 2001.

Coale, K. H., Johnson, K. S., Fitzwater, S. E., Gordon, R. M., Tanner, S., Chavez, F. P., Ferioli, L., Sakamoto, C., Rogers, P., Millero, F., Steinberg, P., Nightingale, P., Cooper, D., Cocklan, W. P., Landry, M. R., Constantinou, J., Rollwagen, G., Trasvina, A., and Kudela, R.: A massive phytoplankton bloom induced by an ecosystem-scale iron fertilization experiment in the equatorial Pacific Ocean, Nature, 383, 495-501, 1996.

Cook, E. R,, Woodhouse, C. A., Eakin, C. M., Meko, D. M., and Stahle, D. W.: Long term aridity changes in the western united states, Science, 306, 1015-1018, 2004.
Denton, G. H., Anderson, R. F., Toggweiler, J. R., Edwards, R. L., Schaefer, J. M., and Putnam, A. E.: The last glacial Termination, Science, 328, 1652-1656, 2010.
Duke, J. H.: A Common Mechanism of Multi-time scale Abrupt Global Change. Eos Trans. AGU, 83(47), Fall Meet. Suppl., Abstract PP23C-1485, 2008.
Fang, Y., Chiang, J. C. H., and Chang, P.: Variation of mean sea surface temperature and modulation of El Niño – Southern Oscillation variance during the past 150 years, Geophys. Res. Lett., 35, L08703, doi:10.1029/2007GL033097, 2008.
Fedorov. A. and Melville, W. K., Kelvin Fronts on the Equatorial Thermocline, J. of Physical Oceanography, 30, 1692-1705, 2000.
Fedorov, A. V., Dekens, P. S., McCarthy, M.., Ravelo, A. C., deMenocal, P. B., Barreiro, M., Pacanowski, R. C., Philander, S. G.: The Pliocene paradox (mechanisms for a permanent El Niño), Science, 312, 1485-1489, 2006.
Ffield , A. and Gordon, A. L., Tidal mixing signatures in the Indonesian Seas. J. Phys. Oceanography 26, 1924-1937, 1996.
Garrett, C. and Kunze, E.: Internal Tide Generation in the Deep Ocean, Annu. Rev. Fluid Mech., 39, 57–87, 2007.
Gergis, J. L. and Fowler, A. M.: A history of ENSO events since A.D. 1525: implications for future climate change, Climatic Change,92, 343–387, 2009.
Gregg, M. C., Peters, H., Wesson, J. C., Oakey, N. S., and Shay, T. J.: Intensive measurements of turbulence and shear in the equatorial undercurrent, Nature 318, 140-144, 1985.
Grodsky, S. A. and Carton, J. A.: Intense surface currents in the tropical Pacific during 1996-1998, J. Geophysical Res., 206(C8), 16 673-16 684, 2001.
Grootes, P. and Stuiver, M.: Oxygen 18/16 variability in Greenland snow and ice with 10^3–10^5 year time resolution, Journal of Geophysical Research, 102(C12), 26455–26470, 1997.
Hanna, E.: Anomalous peak in Antarctic sea-ice area, winter 1998, coincident with ENSO, Geophys. Res. Lett., 28(8), 1595-1598, 2001.
Haug, G. H., Konrad A., Hughen, K. A., Sigman, D. M., Peterson, L. C., Röhl, U.: Southward migration of the intertropical convergence zone through the holocene, Science 293, 1304-1308, 2001.
Hays, J. D., Imbrie, J., and Shackleton, N. J.: Variations in the earth's orbit: Pacemanker of the ice ages. Science 194, 1121-1132, 1976.
Heming, S. R., Heinrich events: Massive late Pleistocene detritus layers of the North Atlantic and their global climate imprint, Rev. Geophys., 42, RG1005, doi:10.1029/2003RG000128, 2004.
Hinnov, L.A., Schulz, M., and Yiou, P.: Interhemispheric space-time attributes of the Dansgaard-Oeschger oscillations between 100 and 0 ka. Quaternary Science Reviews 21 (10), 1213–1228, 2002.
Huybers, P.: Early Pleistocene Glacial Cycles and the Integrated Summer Insolation Forcing, Science 313, 508-511, 2006.
Huybers, P.: Glacial variability over the last two million years: an extended depth-derived age model, continuous obliquity pacing, and the Pleistocene progression, Quaternary Sci. Rev., 26, 37-55, 2007.
Huybers, P. and Wunsch, C.: Obliquity pacing of the late Pleistocene glacial terminations. Nature, 434, 491-494, 2005.
Huybers, P.: Pleistocene glacial variability as a response to chaotic obliquity forcing, Clim. Past., 5, 482-488, 2009.
Jin, F-F.: An Equatorial Ocean Recharge Paradigm for ENSO. Part I: Conceptual Model, J. Atmospheric Sciences, 54, 811-829, 1997a.
Jin, F-F.: An Equatorial Ocean Recharge Paradigm for ENSO. Part II: A Stripped-Down Coupled Model, J. Atmospheric Sciences, 54, 830-847, 1997b.
Johnson, G. C., Sloyan, B. M., Kessler, W.S., and McTaggart, K. E.: Direct measurements of the upper ocean currents and water properties across the tropical Pacific during the 1990s, Progress in Oceanography, 52, 31-61, 2002.

Jones, J. H.: Vertical mixing in the equatorial undercurrent, J. Physical Oceanography, 3, 286-196, 1973.
Keeling, C. W. and Whorf, T. P.: Possible forcing of global temperature by oceanic tides, P. Natl. Acad. Sci. USA, 94,8321-8328, 1997.
Keeling, C. W. and Whorf, T. P.: The 1,800-year oceanic tidal cycle: A Possible cause of rapid climate change, P. Natl. Acad. Sci. USA, 97(8), 3814-3819, 2000.
Kessler, W. S., Johnson, G. C., and Moore, D. W.: Sverdrup and Nonlinear Dynamics of the Pacific Equatorial Currents, J. Physical Oceanography, 33, 9994-1008, 2003.
Koutavas, A. and Lynch-Stieglitz, J.: Variability of the marine ITCZ over the eastern Pacific during the past 30,000 years, in: The Hadley Circulation: Present, Past and Future, Diaz, H. F. and Bradley, R. S. (eds.), Kluwer Academic Publishers, the Netherlands, 347–369, 2005.
Koutavas, A., Lynch-Stieglitz, J., Marchitto Jr., T. M., and Sachs, J. P.: El Niño-like pattern in ice age tropical Pacific sea surface temperature, Science, 297, 226-230, 2002.
Kukla, G. J., Clement, A. C., Cane, M. A., Gavin, J. E, and Zebiac, Z. E.: Last Interglacial and early glacial ENSO, Quaternary Reasearch, 58, 27-32, 2002.
Kukla, G. J. and Gavin, J. E.: Milankovitch climate reinforcements, Global and Planet. Change, 40, 27-48, 2004.
Kukla, J. G. and Gavin, J. E.: Did glacials start with global warming? Quaternary Sci. Rev., 24, 1547-1557, 2005.
Laskar, J., Robutel, P., Joutel, F., Gastineau, M., Correia, A. C. M., and Levrard, B.: A long term numerical solution for the insolation quantities of the Earth, Astronomy and Astrophysics, 428, 261-285, 2004.
Lisiecki, L. E. and Raymo, M. E.: 2005 A Pliocene-Pleistocene stack of 57 globally distributed benthic δ^{18}O records, Paleoceanography, 20, PA1003, DOI:10.10289/2004pa001071, 2005.
Lisiecki, L. E. and Raymo, M. E.: Plio–Pleistocene climate evolution: trends and transitions in glacial cycle dynamics, Quaternary Science Reviews, 26, 56–69, 2007.
Liu, Z., Cleaveland, L. C., and Herbert, T. D.: Early onset and origin of 100-kry cycles in Pleistocene tropical SST records, Earth and Planetary Science Letters, 265, 703-715, 2008.
Lyard, F., Lefevre, F., Letellier, T., Francis, O.: Modelling the global ocean tides: modern insights from FES2004, Ocean Dynamics, 56: 394–415, 2006.
Lyle, M. W., Prahl, F. G., and Sparrow, M.A. Upwelling and productivity changes inferred from a temperature record in the central equatorial Pacific, Nature, 355, 812-815, 1992.
Marshall, S. J. and Clark, P. U.: Basal temperature evolution of North American ice sheets and implications for the 100-kyr cycle, Geophys. Res. Letters, 29(24), doi:10.1029/2002GL015192, 2002.
McPhaden, M. J. : Genesis and evolution of the 1997-98 El Niño, Science, 283, 950-954, 1999.
McPhaden, M. J.: Evolution of the 2002/03 El Niño, Bulletin of the American Meteorological Society, May, 677-695, 2004.
McPhaden, M. J.: ENSO as an integrating concept in earth science, Science 314, 1740-1745, 2006.
Meeus, J: Mathematical astronomy morsels III, William-Bell, Inc. Richmond, VA USA, 2004.
Meyers, G. and Donguy, J-R.: The north equatorial countercurrent and heat storage in the western Pacific Ocean durinh 1982-83, Science 312, 258-260, 1984.
MICA 2.0: US Naval Observatory multiyear Interactive computer almanac 1800-2050, Willmann-Bell, Inc. Richmond, VA, 1998-2005.
Munk, W., Dzieciuch, M., and Jayne, S.: Millennial Climate Variability: Is There a Tidal Connection? J. Climate, 15, 370-385, 2002.
Murray, R. W., Knowlton, C., Leinen, M., Mix, A. C., and Polsky, C. H.: Export production and carbonate dissolution in the central equatorial Pacific Ocean over the last 1 Myr, Paleoceanography, 15(6), 570-592, 2000a.
Murray, R. W., Knowlton, C., Leinen, M., Mix, A. C., and Polsky, C. H.: Export production and terrigenous matter in the Central Equatorial Pacific Ocean during interglacial oxygen isotope Stage 11, Global and Planet. Change, 24, 59-78, 2000b.
Multivariate ENSO Index, Earth Systems Research Laboratory/NOAA (http://www.esrl.noaa.gov/psd/enso/mei/)

NASA Eclipse website at http://eclipse.gsfc.nasa.gov/eclipse.html

Oort, A. H. and Yienger, J. J.: Observed interannual variability in the Hadley Circulation and its connection to ENSO, J. Climate, 9, 2751-2767, 1996.

Ortiz, J. D., O'Connell, S. B., Delvisco, J., Dean, W., Carriquiry, J. D., Marchitto, T., Zheng, Y., and van Geen, A.: Enhanced marine productivity off western North America during warm climate intervals of the past 52 k.y., Geology, 32(6), 521–524, 2004.

Paytan A., Kastner, M., Chavez, F. P.: Glacial to Interglacial Fluctuations in Productivity in the Equatorial Pacific as Indicated by Marine Barite, Science, 274, 1355-1357, 1996.

Pedersen, T. F.: Increased productivity in the eastern equatorial Pacific during the lat glacial maximum (19,000 to 14,000 B.P.), Geology, 11, 16-19, 1983.

Picaut, J., Ioualalen, M., Menkes, C., Delcroix, T., McPhaden, M. J.: Mechanism of the Zonal Displacements of the Pacific Warm Pool: Implications for ENSO, Science, 274, 1486-1489, 1996.

Potter, D., personal communication, 2011: Figure 5c is output from a Morlet transform applied to one hour resolution TAO data prior to 2000, and thereafter sampled at one hour intervals from 10 minute data for consistency. Prior to applying the Morlet transform, missing temperature data was back-filled using a 7 point running median filter followed by a global assignment of the original data set median to all remaining missing data points. See Torrence and Campo (1998) and Bunn (2010) for details on the implementation of the Morlet transform used.

Ray, R. D.: Decadal climate variability: Is there a tidal connection?, J. Climate, 20, 3542-3560, 2007.

Raymo, M.: The timing of major climate terminations, Paleoceanography, 12(4), 577-585, 1997.

Raymo, M. E., and Nisancioglu, K.: The 41 kyr world: Milankovitch's other unsolved mystery, Paleoceanography, 18(1), 1011, doi:10.1029/2002PA00079, 2003.

Ruddiman, W. F.: Orbital changes and climate, Quaternary Sci. Rev., 25, 3092-3112, 2006.

Ryan, J. P., Polito, P. S., Strutton, P. G., and Chavez, F. P.: Unusual large-scale phytoplankton blooms in the equatorial Pacific, Prog. Oceangr., 55, 263-285, 2002. Sachs, J. P., Sachse, D., Smittenberg, R. H., Zhang, Z., Battisti, D. S., and Golubic, S.: Southward movement of the Pacific intertropical convergence zone AD 1400–1850, Nature Geoscience, 2, 519-525, 2009.

Sachs, J. P., Sachse, D., Smittenberg, R. H., Zhang, Z., Battisti, D. S., and Golubic, S.: Southward movement of the Pacific intertropical convergence zone AD 1400–1850, Nature Geoscience, 2, 519-525, 2009.

Sandweiss, D. H., Richardson, J. B. III, Reitz, E. J., Rollins, H. B., Maasch, K. A.: Geoarchaeological evidence from Peru for a 5000 years B. P. onset of El Niño, Science, 273, 1531-1533, 1996.

Schlosser, E., Powers, J. G., Duda, M.G., and Manning, K. W.:Interaction between Antactic sea ice and synoptic activity in the circumpolar trough: implications for ice-core interpretation. Annals of Glaciology, 52(57) 2011.

Seager, R., Naik, N., Ting, M., Cane, M. A., Harnik, N., and Kushnir, Y.: Adjustment of the atmospheric circulation to tropical Pacific SST anomalies: Variability of transient eddy propagation in the Pacific-North America sector, Q. J. R. Meteorol. Soc. 00: 1–26 , 2009.

Seager, R., Clement, A. C., and Cane, M. A.: Glacial Cooling in the Tropics: Exploring the roles of Tropspheric Water Vapor, Surface Wind Speed, and Boundary Layer Proceses, J. Atmos. Sci., 57, 2144-2157, 2000.

Seager, R., Battisti, D. S., Yin, J., Gordon, N., Naiki, N., Clement, A. C. and Cane, M. A.: Is the Gulf Stream responsible for Europe's mild winters?, Quarterly J. Roy. Met. Soc., 128(586), 2563-2586, 2002.

Seidel, D. J., Fu, Q., Randel, W. J., and Reichler, T. J.: Widening the tropical belt in a changing climate, Nature Geoscience, 1, 21-24, 2008.

Solomon, S., Rosenlof, K. H., Portmann, R. W., Daniel, J. S., Davis, S. M., Sanford, T. J., Plattner, G-K.: Contributions of stratospheric water vapor to decadal changes in the rate of global warming, Science, 327, 1219-1223, 2010.

Steffensen, J. P., Anderson, K. K., Bigler, M., Clausen, H.B., Dahl-Jensen, D., Fischer, H., Goto-Azuma, K., Hansson, M., Johnsen. S.J., Jouzel, J., Masson-Delmotte, V., Popp, T., Rasmussen, S. O., Röthlisberger, R., Ruthe, U.,Stauffer, B., Siggaard-Andersen, M-L., Sveinbjorndottir, A.E.,

Svensson, A., White, J. W. C.: High resolution Greenland ice coredata show abrupt climate change happens in few years, Science, 321, 680-684, 2008.
Steves, B. A.: The cycles of selene, Vistas in Astronomy, 41(4), 543-571, 1998.
Stott, L., Poulsen, C., Lund, S., Thunell, R., Super ENSO and global climate oscillations at millennial time scales, Science, 297, 222-226, 2002.
Sverdrup, H. U.: Wind-driven currents in a baroclinic ocean; with application to the equatorial currents of the eastern Pacific, Proc. N. A. S., 33, 318-326, 1947.
Takahashi, T., Sutherland, S. C., Sweeney, C., Poisson, A., Metzl, N., Tilbrook, B., Bates, N., Wanninkhof, R., Feely, R. A., Sabine, C., Olafsson, J., Nojiri, Y.: Global sea-air CO2 flux based on climatological surface ocean pCO2, and seasonal biological and temperature effects, Deep-Sea Res. Pt II, 49, 1601-1622, 2002.
Timmermann, A., Lorenz, S. J., An, S.-I., Clement, A., and Xie, S. -P.: The Effect of Orbital Forcing on the Mean Climate and Variability of the Tropical Pacific, J. Climate, 20(16), 4147-4159, 2007a.
Torrence, C. and Compo, G.P.: A practical guide to wavelet analysis. Bulletin of the American Meteorological Society, 79: 61–7, 1988.
Treolar, N. C.: Luni-solar tidal influences on climate variability, Intl. J. Climatology, 22, 1527-1542, 2002.
Van den Bergh, G.: Periodicity and variability of solar (and lunar) eclipses, H. D. Tjeenk Willink & Zoon N.V., Haarlem, 1955.
Vecchi, G. A.: The Termination of the 1997-1998 El Niño. Part II: Mechanism of Atmospheric Change, J. Climate, 19, 2647-2664, 2006.
Wang, B. and Wang, Y.: Dynamics of the ITCZ-equatorial cold tongue complex and causes of the latitudinal climate asymmetry, J. Climate, 12, 1830-1847, 1999.
Wang, C. and Picaut, J.: Understanding ENSO physics - A review, in Earth's Climate: The Ocean-Atmosphere Interaction, AGU Geophysical Monograph Series 147, 21-48, 2004.
Wang, X., Auler, A. S., Edwards, R. L., Cheng, H., Cristalli, P. S., Smart, P. L., David A. Richards, D. A., and Shen, C-C.: Wet periods in northeastern Brazil over the past 210 kyr linked to distant climate anomalies, Nature, 432, 740-743, 2004.
Wells, M. L., Vallis, G. K., and Silver, E. A.: Tectonic Processes in Papua New Guinea and past productivity in the eastern equatorial Pacific Ocean, Nature, 398, 601-604, 1999.
Wood, F.: Tidal dynamics, Reidel, Dordrecht, the Netherlands, 1986.
Wunsch, C.: Towards understanding the Paleocean, Quaternary Science Reviews 29, 1960-1967, 2010.
Wyrtki, K. and Kilonsky, B.: Mean Water and Current Structure during the Hawaii-to-Tahiti Shuttle Experiment. Journal of Physical Oceanography, 14, 242-254, 1984.
Wyrtki, K.: Water Displacements in the Pacific and the genesis of El Niño cycles, J. Geophysical Research, 90(C4), 7129-7130, 1985.
Xie, S. –P.: The shape of continents, air-sea interaction, and the rising branch of the Hadley Circulation, in: The Hadley Circulation: Present, Past and Future, H.F. Diaz and R.S. Bradley (eds.), Kluwer Academic Publishers, the Netherlands, 121-152, 2005.
Yuan, X.: ENSO-related impacts on Antarctic sea ice: a synthesis of phenomenon and mechanisms, Antarctic Science 16 (4): 415–425, 2004.

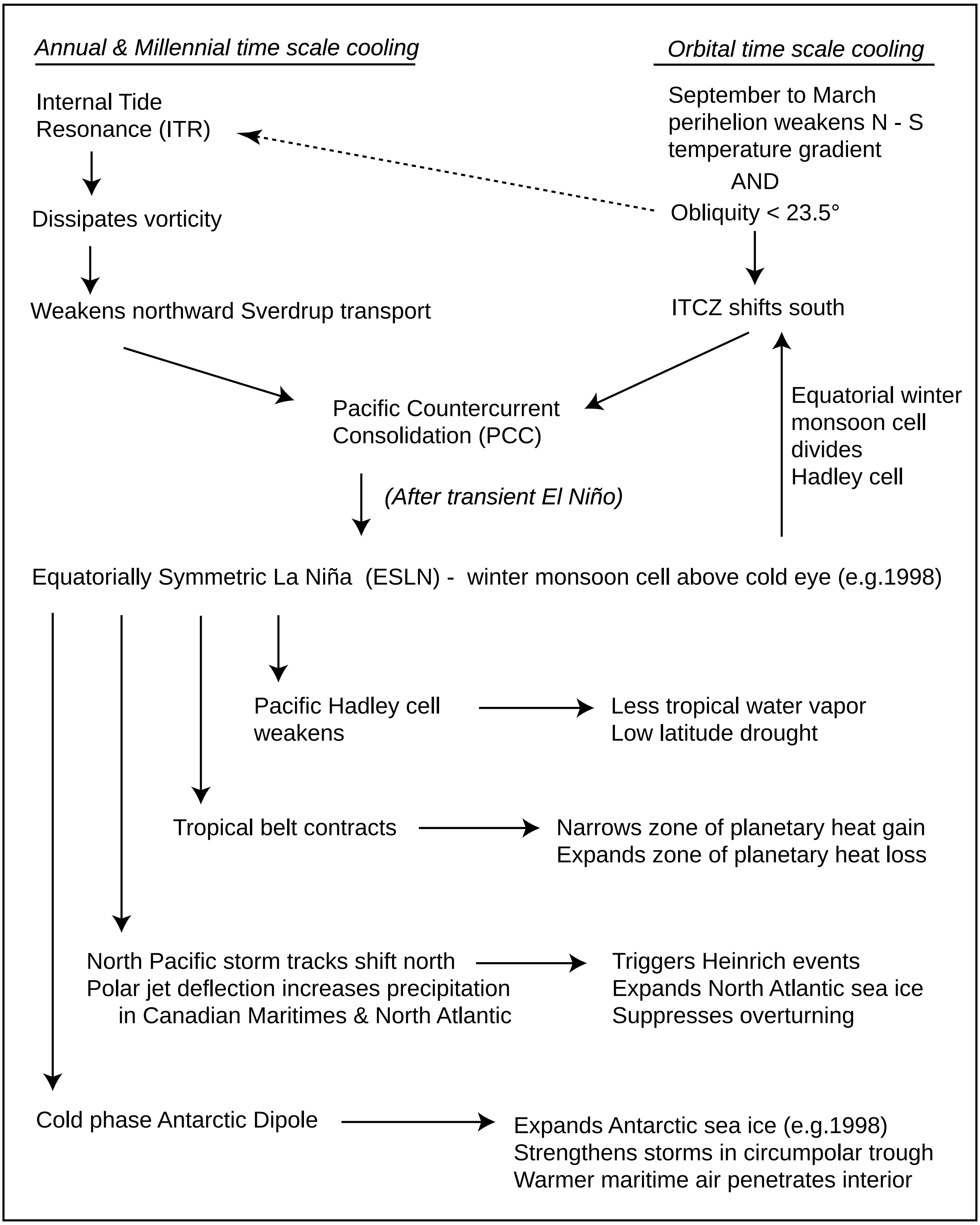

Fig.1. Diagram of proposed integrated time scaleclimate forcing hypothesis.

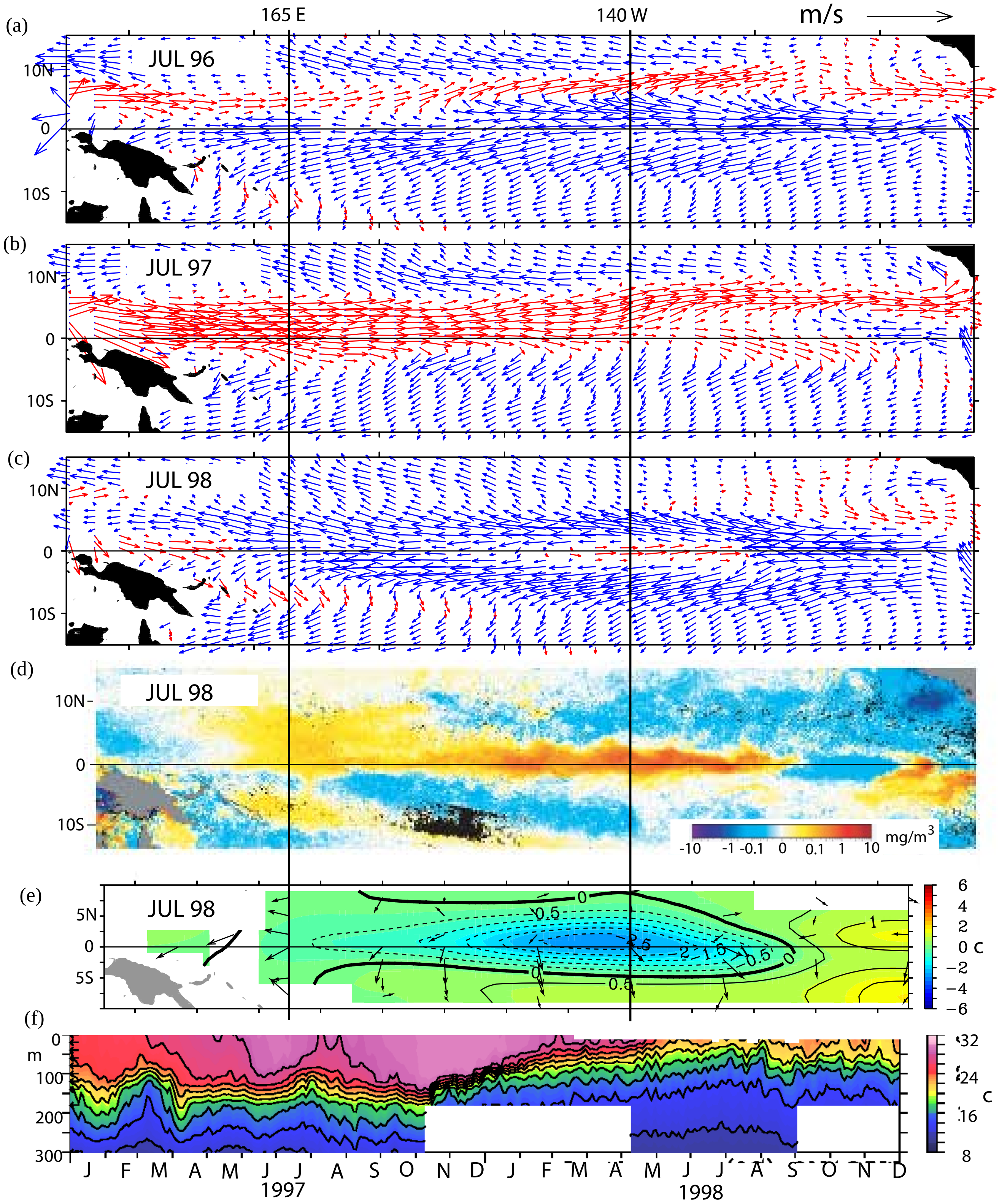

Fig. 2 Mean July surface currents, red eastward, blue westward, for (a) 1996, (b) 1997, (c) 1998. Mean July 1998: (d) Chlorophyll anomaly, (e) Sea surface temperature anomaly, (f) 5 day average isotherms at 0°N 140°W. Sources: OSCAR Project Office, Bonjean and Lagerloef (2002), SeaWiFS Project/NASA, TAO Project Office PMEL/NOAA.

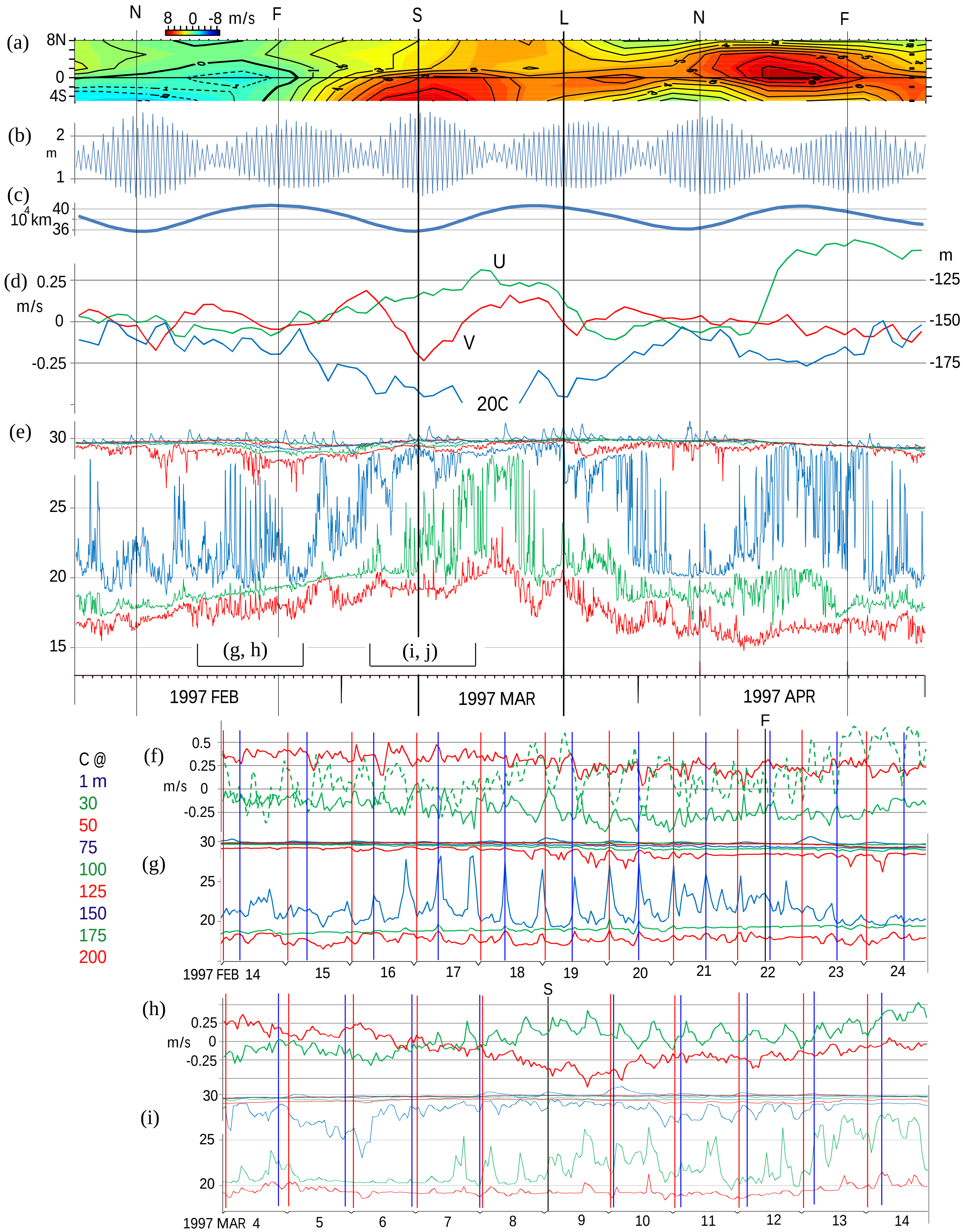

Fig. 3. February to April 1997: (a) 165°E Latitude-Time plot of 5 day mean zonal wind anomaly, (b) Height of tide above datum at Marshal Islands, (c) Lunar distance. At 0°N 165°E: (d) Daily 30-245 m average zonal (green) and meridional (red) current and 20°C isotherm (blue, right scale), (e) One hour resolution subsurface temperatures at depths shown, (f) One hour resolution detail of zonal current at 100 m (solid green), 150 m (dashed green) and meridional current at 100 m (red), (g) Detail of (e), (h) Detail as in (f), (i) Detail of (e), with local meridian passage of moon (blue) and sun (red). Sources: TAO Project Office PMEL/NOAA, CO-OPS/NOAA, MICA.

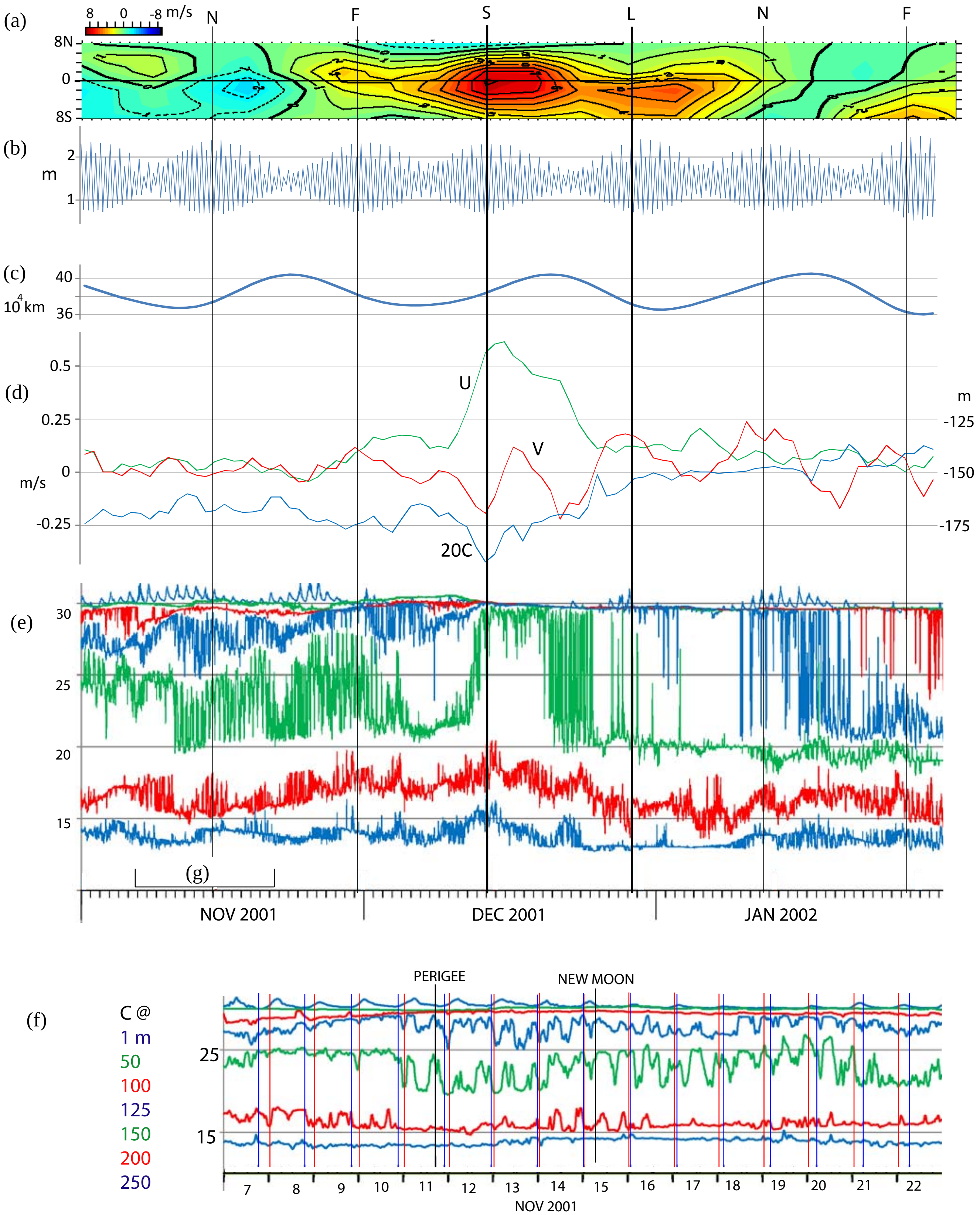

Fig. 4. November 2001 to January 2002: (a-d) as in Fig 1, (e) Ten minute resolution subsurface temperatures at depths shown, (f) Detail of (e), with local meridian passage of moon (blue) and sun (red). Sources: TAO Project Office PMEL/NOAA, CO-OPS/NOAA, MICA.

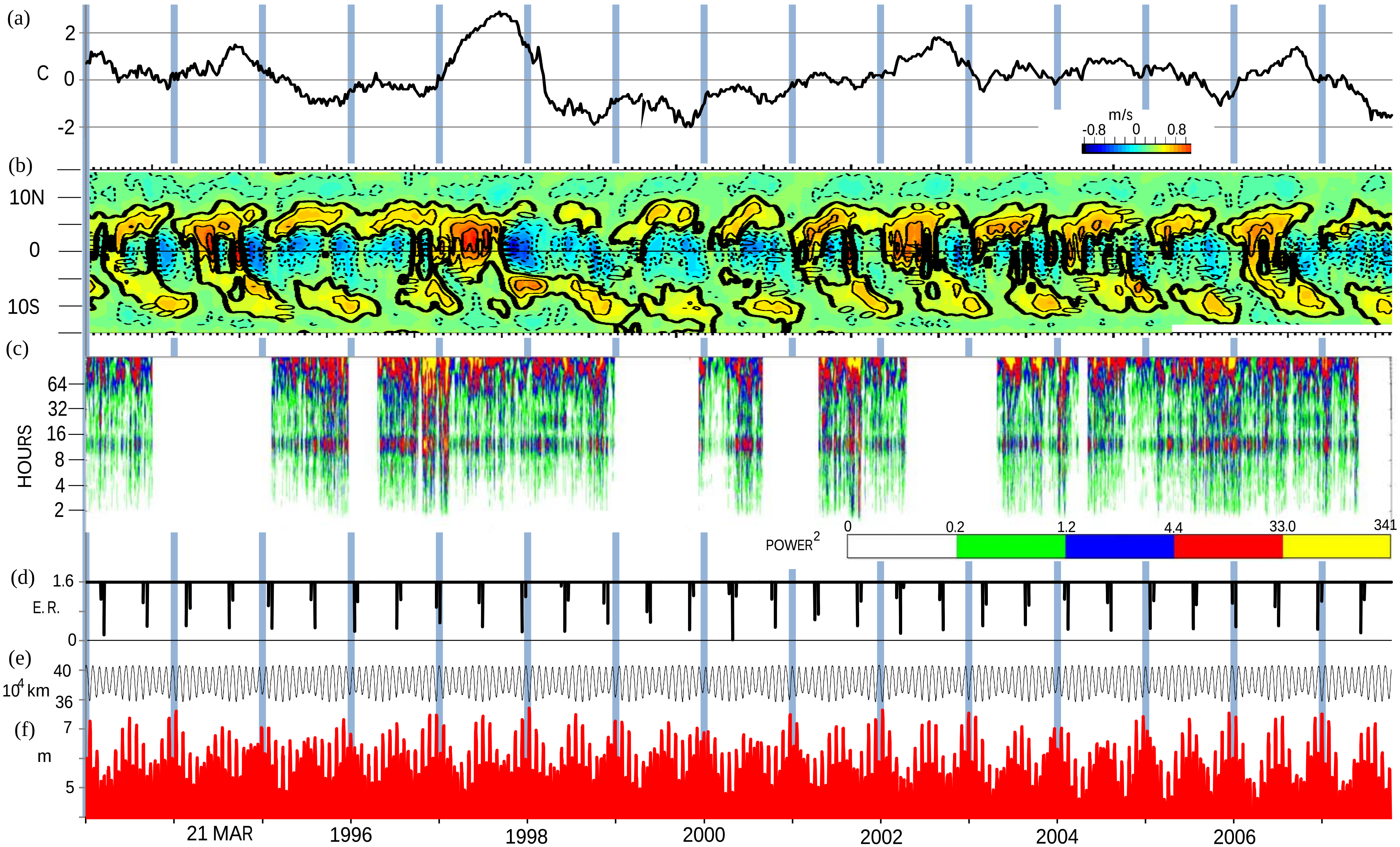

Fig. 5. 1993 to 2011: (a) Weekly Niño 3.4 index, (b) Latitude-Time plot of 5 day average zonal surface current at 165°E, (c) Wavelet analysis of 150 m temperature, (d) Eclipse gamma (e) Lunar distance, and (f) Daily tide displacement at Marshall Islands (see text).
Sources: CPC/NOAA, OSCAR Project Office, Bonjean and Lagerloef (2002), TAO Project Office PMEL/NOAA, MICA, CO-OPS/NOAA.

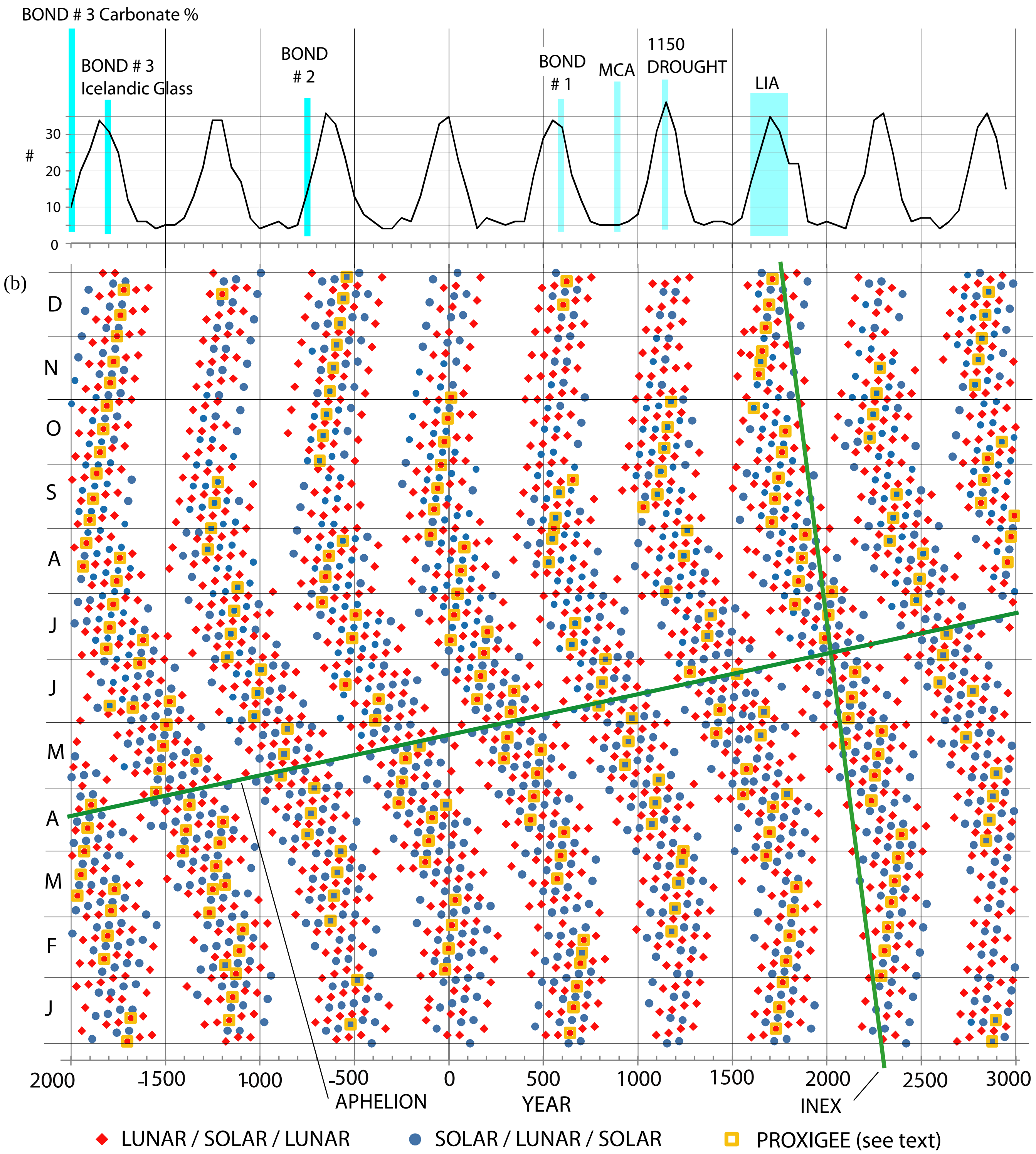

Fig. 6. -2000 to 3000: (a) Sum of eclipses within 50 years following date shown with absolute value of gamma < 0.25; (b) Day-year plot of LGE distribution (see text). Sources: Fred Espenak GSFC/NASA, John Walker Lunar Perigee and Apogee Calculator (www.fourmilab.ch/earthview/pacalc).

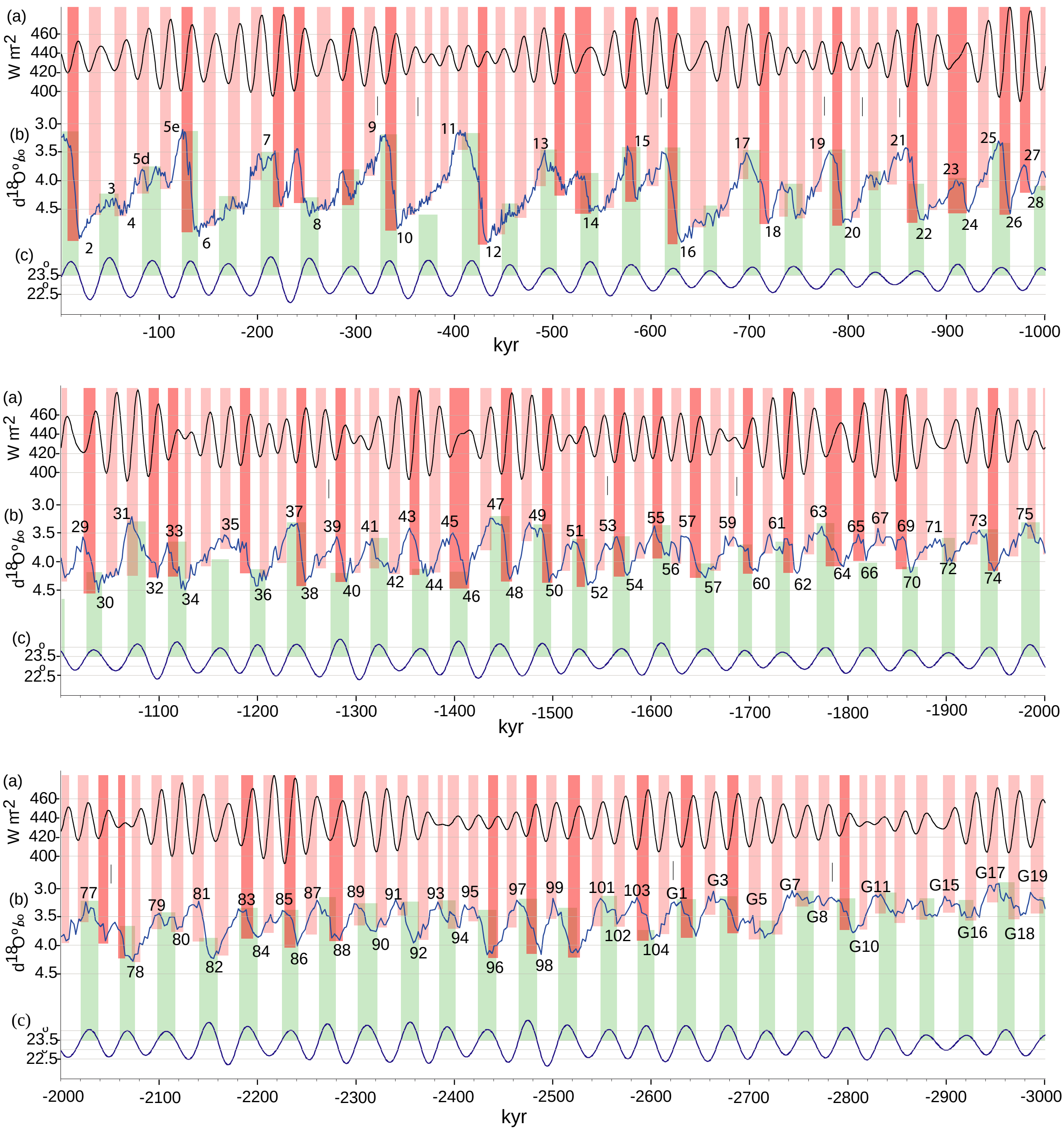

Fig. 7. 3 myr to present: (a) Mid-month March insolation at equator; (b) d18O 0/00; (c) Obliquity. Vertical red shading is between mid-month March perihelion and mid-month September perihelion. Dark red shading is selected fast melt intervals (see text). Vertical green shading is obliquity > 23.5°. Sources: Berger (1978) and Laskar (2004), Lisiecki and Raymo (2005), Berger (1991).